Resistive transition for $YBa_2Cu_3O_{7-\delta}$-Y_2BaCuO_5 composites: Influence of a magnetic field

H. S. Gamchi, G. J. Russell, and K. N. R. Taylor
School of Physics, The University of New South Wales, Sydney, New South Wales 2052, Australia
(Received 14 April 1994)

The resistive transitions of $YBa_2Cu_3O_{7-\delta}$-Y_2BaCuO_5 granular composites (denoted as Y_{123}/Y_{211}) have been systematically investigated under applied magnetic fields up to 4 kG at a fixed low transport current density of 1.5 mA cm^{-2}. In the region of the superconducting transition the samples showed two distinct sections, a steep part associated with the onset of superconductivity in the individual grains and a transition tail due to the weak links coupling the grains. For each composite the steep section remained unchanged with applied field while the tails moved considerably to lower temperatures with this dissipation region being very sensitive to both transport current and applied field as the percolation limit was approached. The resistivity tails have been interpreted using the Ambegaokar and Halperin (AH) phase-slip model and a four-variable fitting procedure. The AH parameter $\gamma(H)_{T=0}$ has been used to estimate the critical current density, at zero temperature, in the grain boundaries for the different composites at various magnetic fields. The magnetic field dependence of $\gamma(H)$ was found to be $\propto H^{-n}$ with $n=0.5$ for pure Y_{123} and 0.3 for the other composites. The resistivity data near T_c ($\rho=0$) did not conform with the AH model and have been interpreted in terms of the thermally activated flux-creep model. Pinning energies have been determined and were also found to follow the applied magnetic field according to $H^{-\alpha}$ with $\alpha=0.60$ for all composites.

INTRODUCTION

Since the discovery of high-T_c superconductivity, the broadening of the resistive transitions for these materials by both magnetic fields and transport currents has been the subject of extensive studies. Some workers, Batlogg *et al.*,[1] Palstra and co-workers,[2,3] Malozemoff *et al.*,[4] and Griessen[5] pointed out that a thermally activated flux-creep model can describe the broadening behavior quite well for the resistivity region near T_c ($\rho=0$). These groups found a temperature-independent activation energy U_0, and obtained a very weak-field-dependent energy barrier from the slopes of Arrhenius resistivity plots, involving $\rho=\rho_0\exp[-U_0(H)/T]$. The physical picture here separates a thermally activated flux-creep regime at low temperatures, where $U_0 \gg k_B T$ (Ref. 6) from a viscous flux-flow regime where thermal energies become comparable to barrier energies and the Lorentz force dominates.[7,8] The origin of this model is based on the balance of two opposing forces acting on the flux-line lattice, namely, the pinning force due to spatial variations of the condensation energy and the macroscopic Lorentz force exerted by a transport current of density J in the presence of a magnetic flux density B ($F_d=J\times B$). Extensive studies in the past have revealed the distinct characteristics for both regimes.[9–12]

However, some recent measurements[13–18] of the resistive transitions in the highly anisotropic high-T_c superconductors, $Bi_2Sr_2CaCu_2O_x$, $(La,Sr)_2CuO_4$, $Tl_2Ba_2CaCu_2O_x$, and $YBa_2Cu_3O_{7-\delta}$ systems show that the major component of the thermally activated resistivity in the high-T_c materials is insensitive to the orientation between the field and current as long as they are in the same plane, the macroscopic Lorentz force playing only a minor role in this loss mechanism.[14,18] Since the Lorentz force is essential to an understanding of such losses in terms of magnetic-flux motion, these measurements cast doubt on the interpretation of thermally activated dissipation in terms of flux creep.

Other workers, however, have made various attempts to find the origin of this contradiction. Explanations based on flux cutting[19] or deviations of the microscopic current from its macroscopic direction (the introduction of a microscopic Lorentz force and flux motion) cannot explain the virtual equivalence of the results for magnetic fields applied parallel and perpendicular to the current flow direction.

An alternative approach to the problem of flux-line lattice motion in a magnetic field leading to induced dissipation behavior of the high-T_c oxides has been achieved by applying the phase-slip model of Ambegaokar and Halperin[20] (AH) to a medium of Josephson weak links, regarded as a single effective junction, as originally suggested by Tinkham and Lobb.[21,22] The AH theory describes the effects of thermal fluctuation of the phases of the order parameters across a highly damped, current-driven Josephson junction. Both granular and single-crystal high-T_c superconductors have been examined with this model[21–25] and good agreement has been found between experimental data and theory.

Using material of nominal compositions $Y_{1.x}$, where x indicates the Y_{123}:Y_{211} ratio, with $0\le x\le 1$, we have measured the magnetoresistance as a function of temperature under various applied magnetic fields. These measurements, which support the view that polycrystalline $YBa_2Cu_3O_{7-\delta}$ system is a weakly coupled granular superconductor, suggest that the onset of superconductivity in these materials occurs via a dynamical process whose behavior is substantially more complex than a classical

thermally activated flux-creep process, which simply gives a temperature-independent activation energy for flux motion.

In zero magnetic field, we find that the development of a fully superconducting state in this system occurs via an intermediate phase bounded from above by a zero-resistance temperature, denoted by T_{c1}, and from below by a zero-dissipation temperature T_{c0}. Above T_{c1} the materials exhibit the resistive transition of a conventional fluctuation-broadened superconductor.[26] This broadened resistive transition is associated with the onset of superconductivity in individual grains.

We have found that for an individual composite the nature of the transition in the dissipation regime is strongly influenced by weak externally-applied magnetic fields. However, the superconducting transition width of the initially steep component remains unaffected by a magnetic field over the range $0<H<4$ kG with increasing concentration of the Y_{211} phase in the $Y_{1.x}$ system, while the resistivity tails of the samples become very sensitive to the applied fields.

In this work the observed dissipation from a weakly coupled array of grains, as found in the different composite samples, has been fitted to the AH model using the equation[22]

$$\rho/\rho_n=[I_0(\gamma_0/2)]^{-2} \tag{1}$$

for the field-induced resistivity. Here, ρ_n is the average normal-state resistivity of the junctions, I_0 is the modified Bessel function, and γ_0 is a normalized barrier height, considered to be the same value for all the links in the network, defined as

$$\gamma_0=U_0/k_BT=A(1-t)^{3/2}/H\ . \tag{2}$$

U_0 is the barrier height, H the applied magnetic field, t the reduced temperature, T/T_c and the factor $A=3.5\beta J_{c0}(0)$, for the $YBa_2Cu_3O_{7-\delta}$ (YBCO) system with $T_c=92$ K, $\beta\sim1$ and $J_{c0}(0)$ the critical current density at $T=0$ and $H=0$.

Equation (1) has been fitted successfully to YBCO single crystal data by Tinkham[22] using A as a single fitting parameter. Wright, Zhang, and Erbil[23] have also fitted data from magnetoresistance measurements of the polycrystalline Bi-Pb-Sr-Ca-Cu-O system to this function with A and T_c as two adjustable parameters and found that the results agreed well with predictions of this model.

However, we let $\gamma_0=A(1-t)^q/H$ in Eq. (2), as the exponent q, which had been defined to be 3/2 by Tinkham,[22] is taken as a fitting parameter to be determined empirically. This arises as Deutscher and Müller[27] suggested q should be 2, while Kim *et al.*[28] found q to be in the range 1.53–2.8 for their experimental data. The results of this interpretation for the resistive tails give rise to a temperature and magnetic field dependent phase-slip activation energy $U_0(T,H)$ for weakly coupled Josephson junctions as discussed below.

SAMPLE PREPARATION AND CHARACTERIZATION

Mixed two-phase composite samples consisting of Y_{123} and Y_{211} were fabricated by sintering various compositions determined from the tie line joining the Y_{123} and Y_{211} point compounds in the CuO-Y_2O_3-$BaCO_3$ compositional diagram. In this process the composite samples lay between the two well-known superconducting Y_{123} and

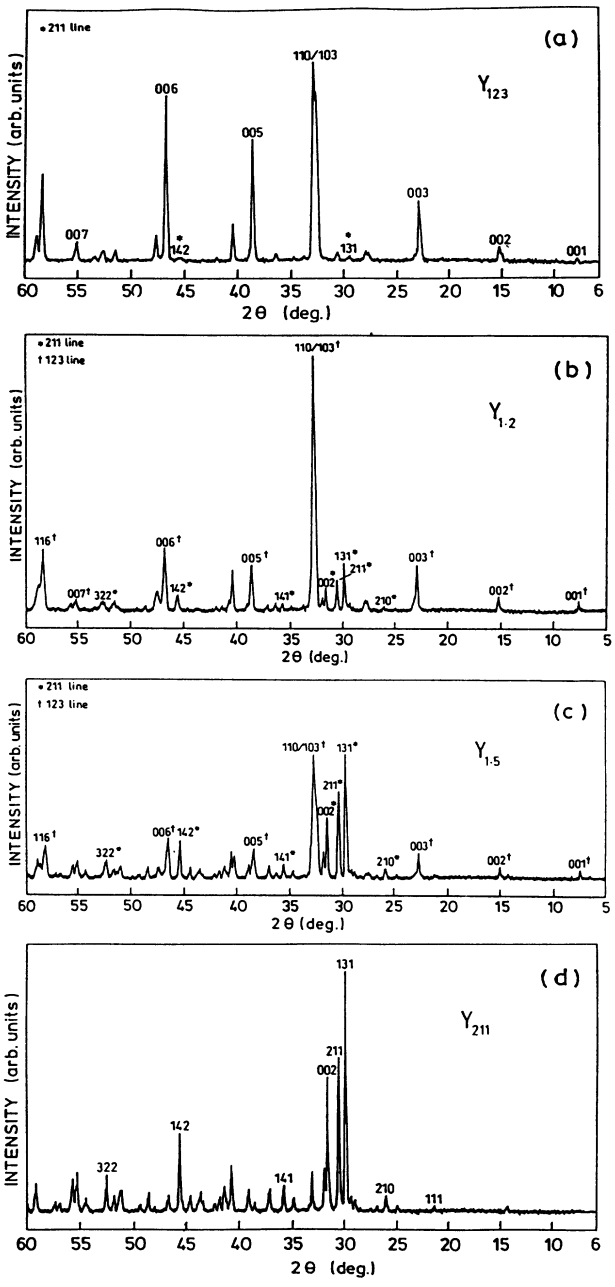

FIG. 1. X-ray-diffraction patterns of different granular samples used in this study. (a) "Pure" $YBa_2Cu_3O_{7-\delta}$ phase with two high-intensity lines of the Y_{211} phase shown. (b) The $Y_{1.2}$ composite showing a decrease in the intensity of the Y_{123} lines and increase in the intensity of the Y_{211} lines. (c) The $Y_{1.5}$ composite showing the significant increase in the Y_{211} phase. (d) The pure Y_2BaCuO_5 phase.

insulating Y_{211} phases. These samples can hereafter be identified by their yttrium stoichiometry, since this value fully identifies the position of the composite on the tie line and hence the composition ratio Y_{123}:Y_{211}. Therefore, for example, the sample with 30% Y_{211} will be called $Y_{1.3}$.

All the samples were prepared using the well-known and documented solid-state reaction method. Stoichiometric amounts of the starting materials for the samples along the tie line were determined by considering the appropriate amounts of Y_2O_3, $BaCO_3$, and CuO powder for the Y_{123} and Y_{211} compounds. The homogeneously mixed and pelletized samples were sintered using two different cycles. In the first cycle, the samples were heated to 720 °C at a rate of 120 °C/h and then reacted at 720 °C for 12 h. This was followed by heating to 930 °C at a rate of 120 °C/h and then annealed at 930 °C for 12 h. For the second cycle, the regrounded samples were pressed into pellets of 30-mm diam, approximate thickness 2.6–3.0 mm using a pressure of 600 bars. The pellets were then heated to 930 °C at a rate of 90 °C/h, and then reacted at this temperature for 24 h. Finally, the temperature was decreased to 720 °C at the rate of 20 °C/h and then furnace-cooled to room temperature in flowing oxygen at a cooling rate of 10 °C/h.

X-ray-diffraction (XRD) studies were carried out in order to determine the oxygen content, the impurities, and the distribution of the two different phases in the composite samples. XRD patterns for pure Y_{123}, pure Y_{211}, and two of the $Y_{1.x}$ composite samples are shown in Fig. 1.

Scanning-electron-microscopy (SEM) micrograph studies of the $Y_{1.x}$ composites revealed that the existence of the Y_{211} phase in the system seriously prevents the growth of Y_{123} superconducting clusters, which are responsible for the electrical and magnetic behavior of the composites. With increasing x the superconducting clusters embedded in the insulating phase become smaller so that at a certain value of x all the series-connected current carrying clusters break down causing superconductivity to die away, and this leads to a dramatic change in the normal-state resistivity of the sample.

Typical SEM micrographs of the $Y_{1.x}$ samples are shown in Fig. 2. In these pictures, the light areas indicate the superconducting metallic regions, while the dark areas correspond to the insulating Y_{211} phase. The characteristic features of the micrographs are as follows: For the Y_{123}-rich compositions the superconducting phase forms a continuum containing a dispersion of amorphous insulating Y_{211} particles. With increasing insulating phase in the composition, the superconducting phase forms a labyrinth structure. In these compositions the existence of a high-volume fraction of insulating particles prevents the formation of a continuous metallic region throughout the sample. With further increases in the molar fraction of the insulating phase, the series-connected conduction path lengths, referred to as percolation channels, diminish [Fig. 2(c)]. Meanwhile, the fine Y_{211} particles obviously increase the separation of the large crystalline grains. Finally, in high Y_{211} concentration samples a complete matrix inversion takes place so that the insulating phase now forms a continuum and the superconducting particles are dispersed throughout the matrix [Fig. 2(d)].

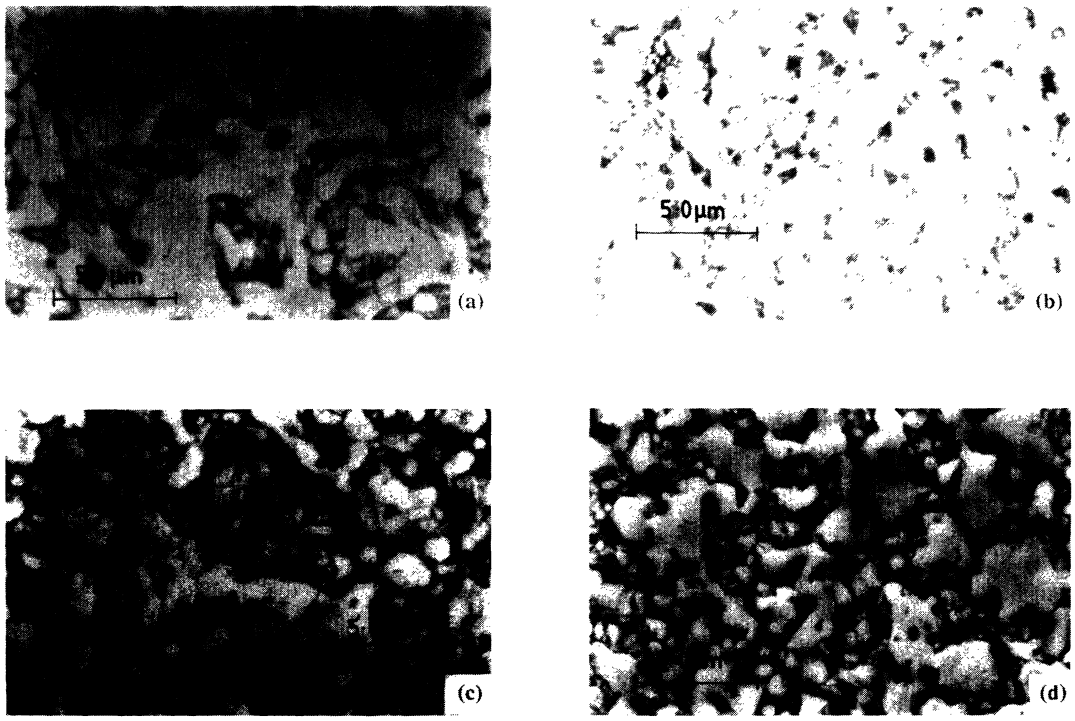

FIG. 2. High-resolution SEM micrographs of (a) the $Y_{1.2}$, (b) the $Y_{1.4}$, (c) the $Y_{1.6}$, and (d) the $Y_{1.775}$ composite samples showing granular decrease of the superconducting cluster size (light areas) as the Y_{211} concentration increases.

Since the oxygen content of the samples plays a crucial role on the transition temperature, the electrical and magnetic behavior of the YBCO system, the oxygen content was evaluated using a method based on the linear relationship between the c-axis lattice parameter and the oxygen content of the orthorhombic YBCO phase.[29] Using this method the oxygen content of the different samples was found to be very similar with a variation between 6.86 and 7.0.

RESULTS AND DISCUSSION

In order to establish the resistive broadening behavior in the $Y_{1.x}$ composites, we have measured the resistive transition of these materials under low-magnetic fields ranging in strength from 0–4 kG. Figures 3(a) and 3(b) show two examples of the magnetoresistance measurements as a function of temperature for a fixed transport current of $I=0.5$ mA. For both composites, $Y_{1.2}$ and $Y_{1.5}$, the application of magnetic fields lower than 4 kG produces virtually a magnetic-field-independent steep drop in the resistivity curves at $T=91.5$ K and a transition tail, which is magnetic field dependent. It is clear from these figures that such a low field only affects the resistivity tails and does not measurably influence the main, steep, part of the resistive transition for an individual composite.

For all the $Y_{1.x}$ composites with $0 \leq x \leq x_c$, where x_c is the percolation limit of this system, which has the experimentally determined value of 0.775,[30] the onset temperature T_c of the superconducting grains remains unaffected (the $Y_{1.2}$ and the $Y_{1.5}$ composites are an example) while for an individual sample the zero resistive temperature T_{c0} of the sample moves to considerably lower temperatures as the applied magnetic field is increased. However, the field-induced broadening greatly increases as the Y_{211} phase is increased in the samples. Figures 4(a) and 4(b) show examples of the enhancement of the resistive tails in

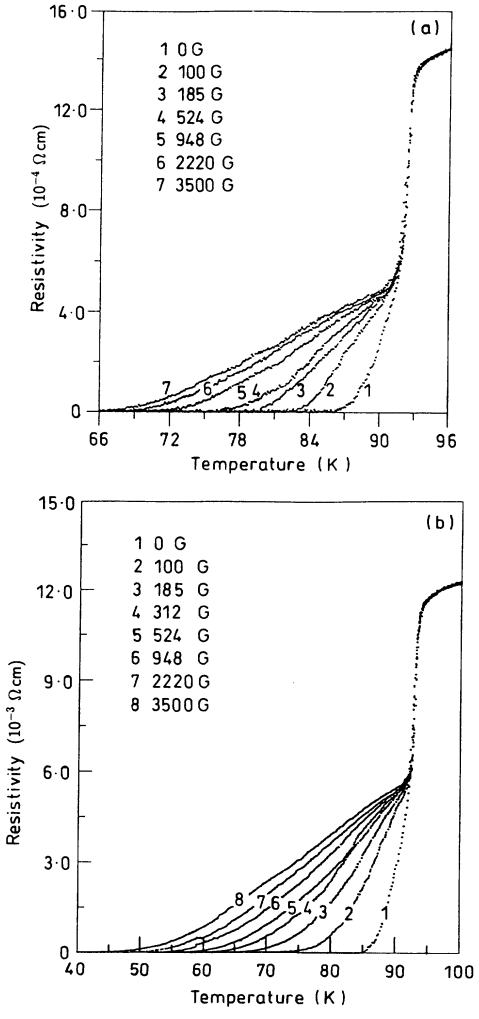

FIG. 3. Resistive transition at different magnetic field values for (a) the $Y_{1.2}$ and (b) the $Y_{1.5}$ composites. These curves show distinct regions: a steep section, associated with the onset of superconductivity in the grains, which is unaffected by the magnetic fields used, and resistive tails, which are sensitive to the applied field.

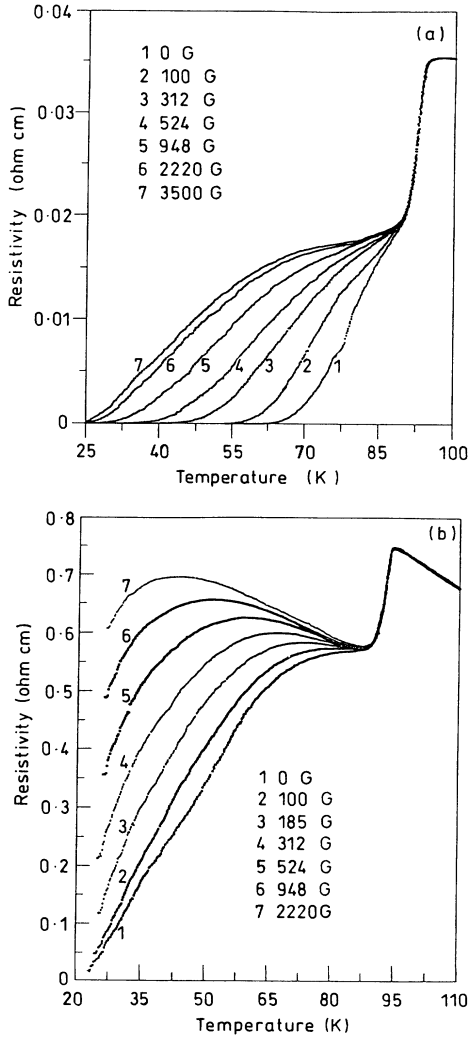

FIG. 4. The magnetoresistivity as a function of temperature for (a) the $Y_{1.6}$ and (b) the $Y_{1.7}$ composites. These curves are similar to those shown in Fig. 3 except for the $Y_{1.7}$ composite at fields greater than 185 G, which destroys the coupling between the superconducting grains.

the high Y_{211} content $Y_{1.6}$ and $Y_{1.7}$ composites, respectively. Since the resistive tails move to temperatures lower than the temperature limit accessible for these measurements, it was not possible to determine the zero resistive-state temperature T_{c0} of the composites with $0.65 \leq x \leq x_c$ in applied magnetic fields.

In order to fit the experimental $\rho(T)$ data for the $Y_{1.x}$ composites to Eq. (1), where γ_0 is given by the modified form, a four-, three-, two-, and one-parameter fitting program was written. To simplify the fitting process, we chose $\gamma_0 = C(1-t)^q$, where $C = A/2H$ is a magnetic field-dependent parameter. Since, for every sample, the value of ρ_n and the corresponding temperature at the onset point of the resistivity tails are field independent and were easily measured for an individual composite, it was anticipated that these parameters could be determined from the experimental data without using them as unknowns in the fitting procedure. However, these composites involve a double-transition system characteristic of the resistive transitions of granular materials,[31] two-dimensional Josephson junctions,[32] and proximity-coupled superconducting arrays.[33,34] Consequently, in order to avoid the ambiguity of the double transition during the fitting process, all fitting of the resistivities excluded the higher-temperature transition, which corresponds to the transition of the superconducting grains. As the $\rho(T)$ curves were well separated at various magnetic fields for the $Y_{1.2}$ composite and the closeness of this sample to the pure Y_{123} composition we first examined the resistivity data of this sample using the AH model.

For the resistivity curves of the $Y_{1.2}$ composite the initial fitting procedure started by using the resistivity and temperature of the branching point of the curves as fixed values for ρ_n and T_c, respectively, while the other two parameters were left free. It was found that these values did not work well when fitting the data at any values of $q > 1$. Using the high-field data, which are more sensitive to both ρ_n and T_c, we established a fixed value for T_c of 92.5 K and $\rho_n = 0.52$ mΩ cm. The value obtained for T_c is close to that of the onset temperature of the superconducting grains and the value of ρ_n is slightly lower than the average value of the resistivity at the branching point of the curves. The value of T_c is unaffected by the field, while ρ_n remains constant for the different fields to within $\pm 2\%$. At the next step we determined the values of the exponent q and the factor C. In order to compare the derived values of C in different magnetic fields we had to keep the exponent q constant and leave C free as a final fitting parameter. However, to obtain a good fitting result with an acceptable standard deviation for the different fields the exponent $q(H) = 1.1$–1.2 for the $Y_{1.2}$ sample. This exponent value is not unique as has been suggested by other workers[35,36] and a similar value is also found for granular NbN films.[37] The results of the fitting procedure (solid lines) and the original experimental $\rho(T)$ curves of this sample are shown in Fig. 5(a). It is clear that the agreement of the data with the AH model is good, except for the low-temperature region, which requires an alternative explanation. The derived values of

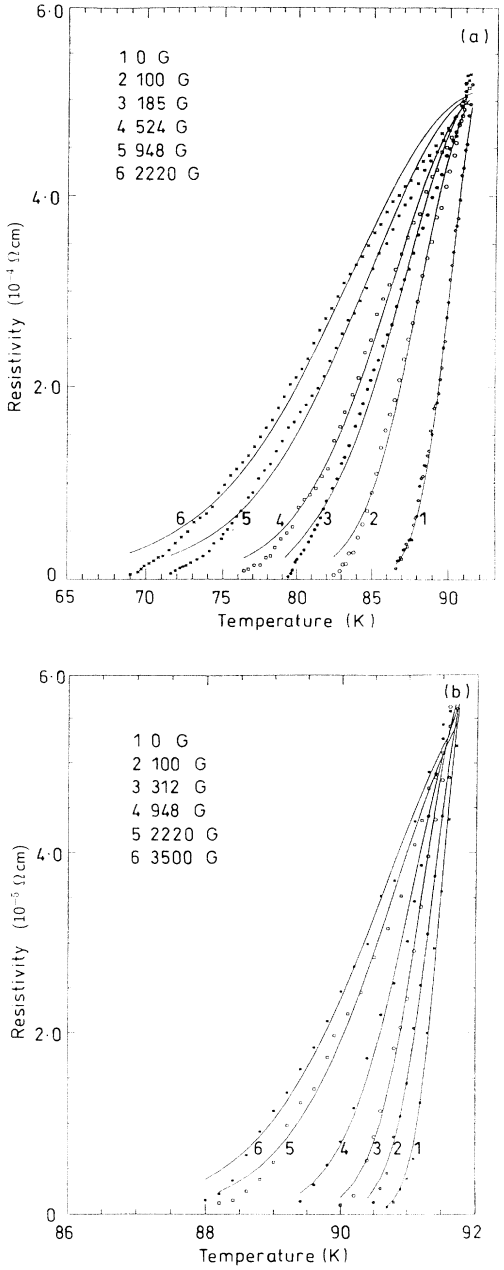

FIG. 5. The points show the temperature dependence of the experimental resistive transition for (a) the $Y_{1.2}$ and (b) the Y_{123} samples at different magnetic fields. The solid lines were obtained by fitting Eq. (1) to the data. (The curves have been truncated at the onset of dissipation.)

$C(H)$ for the $Y_{1.2}$ sample are shown in Table I. The fitting process was continued for the pure Y_{123} and some of the other composites in the $Y_{1.x}$ system. In the case of Y_{123} the value of the exponent q was 1.2–1.25 which is very close to that determined for the $Y_{1.2}$ sample. The fitting also yielded $T_c = 92.5$ K and $\rho_n = 62$ $\mu\Omega$ cm for this sample. These values were almost unaffected by applied magnetic fields (to within $\pm 0.3\%$). As with the $Y_{1.2}$ sample, the value of T_c is very close to the onset tempera-

TABLE I. Values of the parameter $\gamma(H)_{T=0}[C(H)=A/2H]$ from the AH model for several granular $Y_{1.x}$ composites.

Applied magnetic field (G)	Composite	$\gamma(H)$ at $T=0$ Y_{123}	$Y_{1.2}$	$Y_{1.5}$	$Y_{1.6}$
0		780	81	54	15.1
100		470	50	21.4	11.3
185			25.5	14.4	9.8
312		340	21.1	11.4	8.0
524			19	9.3	6.2
948		205	15.2	8.1	5.6
2220		125	12.7	7.4	4.5
3500		97	11.7	6.5	

ture of the superconducting grains. For the Y_{123} sample the value of ρ_n is the same as the resistivity at the branching point of the curves and, of course, is smaller than the normal-state resistivity of the bulk sample at the onset temperature of superconductivity. Figure 5(b) shows the $\rho(T)$ experimental data for the Y_{123} sample together with the fitted curves using Eq. (1).

For the resistivity data of the $Y_{1.5}$ and the $Y_{1.6}$ samples the value of q was found to be in the range 1.1–1.3, which is essentially the same as those found for the other two samples. The fitting procedure yielded the average values of T_c and ρ_n for the $Y_{1.5}$ and the $Y_{1.6}$ composites as 92.9 K and 5.2 mΩ cm and 92.1 K and 18.0 mΩ cm, respectively. Figures 6(a) and 6(b) show the experimental resistivity data and the fitted curves for the $Y_{1.5}$ and the $Y_{1.6}$ composites. The derived curves for the $Y_{1.5}$ sample are satisfactory, while in the case of $Y_{1.6}$ the derived curves show deviation from the experimental data especially at high magnetic fields. The values of $C(H)$ for the Y_{123}, the $Y_{1.5}$, and the $Y_{1.6}$ composites are also tabulated in Table I.

Our results for q are always in complete agreement with that found recently by Gaffney, Petersen, and Bedner[25] for granular YBCO samples and suggest that q is always less than 3/2. A possible reason for this may be associated with the long tail in the transition curves of these samples, which always approaches the zero-resistivity state over a rather long temperature interval. We have also found that for low magnetic fields and large Y_{123} component samples the exponent q tended to slightly higher values, which is not only a source of error for constant q value in our fitting process but suggests that the temperature-dependent activation energy not only depends on the applied magnetic field (as found in Ref. 28), but is also material dependent. These results are consistent with a distribution of Josephson coupling energies for the weak links.

From the AH phase-slip theory, the parameter $C(H)$, which is proportional to the activation energy U, at temperatures close to T_c, is given by

$$C=\frac{J_{cj}(0)\hbar a^2}{ek_BT_c}\ , \tag{3}$$

where $J_{cj}(0)$ is the critical current density at zero temper-

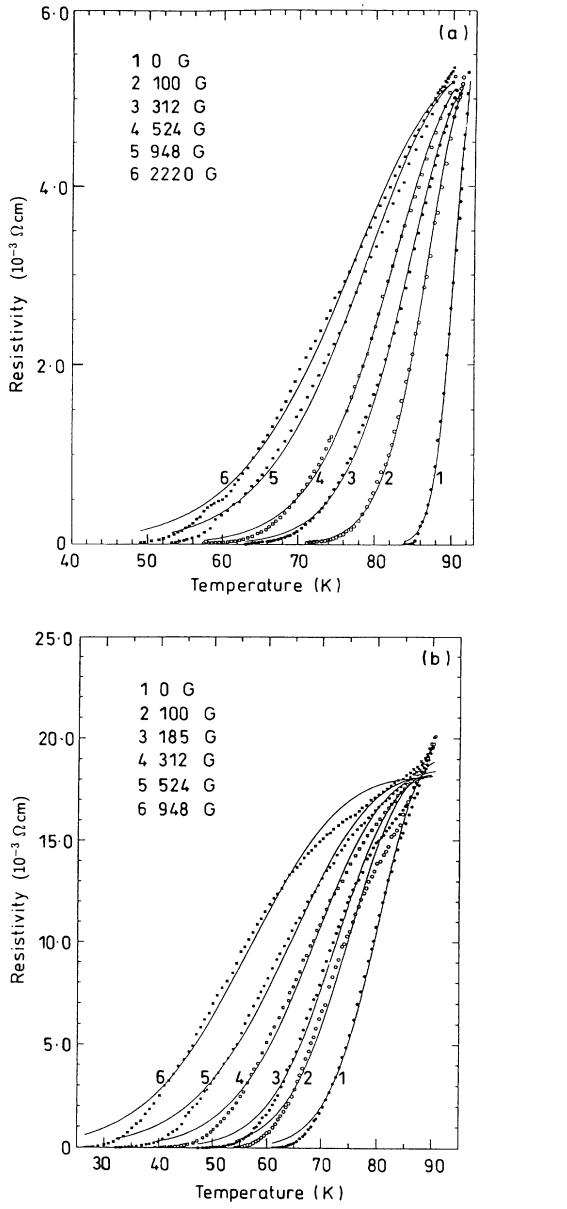

FIG. 6. Curves similar to those of Fig. 5 for (a) the $Y_{1.5}$ and (b) the $Y_{1.6}$ composite samples.

TABLE II. Zero-temperature critical current density, $J_{cj}(0)$, for several $Y_{1.x}$ granular composites.

Applied magnetic field (G)	Composite	$J_{cj}(0)$ (10^3 A cm^{-2}) Y_{123}	$Y_{1.2}$	$Y_{1.5}$	$Y_{1.6}$
100		90.1	9.7	4.2	1.5
185			5.0	2.8	1.3
312		70.0	4.1	2.2	1.0
524			3.8	1.7	0.8
948		39.8	2.9	1.6	0.7
2220		23.7	2.5	1.4	0.6
3500		18.5	2.3	1.3	

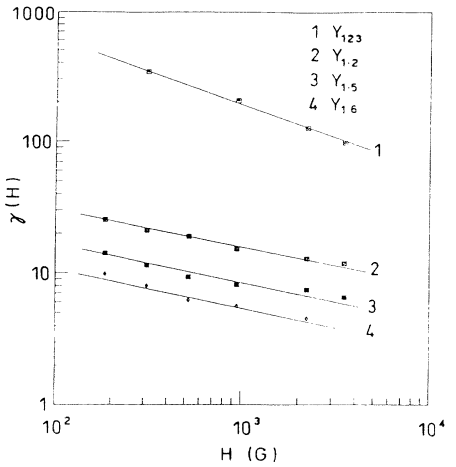

FIG. 7. The magnetic-field dependence of the parameter $\gamma(H)$ as determined form the resistivity data for the $Y_{1.x}$ composites using the AH model.

ature and a is the average grain size. According to this model the value of the critical current in a single Josephson junction, and therefore γ, changes with applied magnetic field. Considering the typical grain size in our samples to be ~ 1 μm and using Eq. (3) we have estimated the values of $J_{cj}(0)$ for the $Y_{1.x}$ composites in various magnetic fields and these are listed in Table II. These values of $J_{cj}(0)$ show that the critical current in the grain boundaries significantly decreases as the Y_{211} concentration is increased in the samples, which in turn is evidence for the sensitivity of a single junction between the superconducting grains to the applied magnetic field in the $YBa_2Cu_3O_{7-\delta}$ compound.

Finally, in order to examine the magnetic field dependence of the parameter γ in our composites, we have plotted, in Fig. 7, the values of $\gamma(H)$ at zero temperature as a function of magnetic field for all the samples. As is evident from this plot, elimination of the data point corresponding to the lowest applied magnetic field for several of the composites, the $\gamma(H)$ data can be easily fitted to a H^{-n} power law. The value of n is then found to be 0.5 for pure Y_{123} and 0.3 for the other $Y_{1.x}$ composites.

The experimental $\rho(T)$ data for the $Y_{1.x}$ composites in the low-temperature region, close to T_{c0}, show a significant deviation from the derived curves using the AH model. In this region the resistivity of the samples is generally $<6\%$ ρ_n. However, the agreement between the two curves for temperatures $> T_{c0}$ is excellent and is consistent with that found by Tinkham for the broadened resistive transitions, under various magnetic fields, for single crystal $YBa_2Cu_3O_{7-\delta}$ samples, in the resistivity region where $\rho(T) > 1\%$ ρ_n.

INTERPRETATION OF RESISTIVITY CURVES NEAR T_{c0} IN TERMS OF THERMALLY ACTIVATED FLUX-CREEP MODEL

The observed deviation of the resistive transition from the derived AH curves for temperatures close to T_{c0} may originate from a different dissipative process. Therefore, we have examined the thermally activated flux-creep model as a means of interpreting our broadened resistivity data in this region.

In the framework of this model, which is an alternative to the Josephson-coupling model, the broadened resistivity curves for the high-T_c oxides can be expressed as[27,37–39]

$$\rho(T,H)=\rho_0 \exp\left[\frac{-U(T,H)}{T}\right] . \tag{4}$$

The resistivity of the material shows a thermally activated behavior with activation energy $U(T,H)$, that is both temperature and magnetic field dependent. The temperature dependent form of the activation energy is assumed to be $U_0(H)(1-t)^q$ with $t=T/T_c$ and $q=1.5$,[22,37–39] 2,[27,40] or 1.0,[35,36] for the high-temperature-superconducting materials.

The resistive transitions for the $Y_{1.2}$ composite have been plotted in Fig. 8 as a function of $(1-T/T_c)^q/T$, where $q=2$ and $T_c=91.5$ (the onset temperature of the broadening point). This Arrhenius plot shows that the resistivity at low temperatures is thermally activated over two orders of magnitude, that is, in the range of $\rho(T)/\rho_n = 10^{-1}$–10^{-3}. It should be noted that we have considered the resistivity of the sample at the branching point of the $\rho(T,H)$ curves as the normal-state resistivity for intergranular material and further that this value is constant for all the applied magnetic fields used.

The slopes of the straight lines shown in Fig. 8 give activation energies, $U_0(H)$, for the flux lines in different magnetic fields and these energies are observed to steadily decrease as the magnetic field strength increases. Further, the preexponential factor, ρ_0, is field independent and almost constant for the resistivity curves of this sample in the various applied magnetic fields. Its value is $(1.0\pm0.2)\times10^{-3}$ Ω cm, which is twice as large as the normal-state resistivity for intergranular material and 1.5

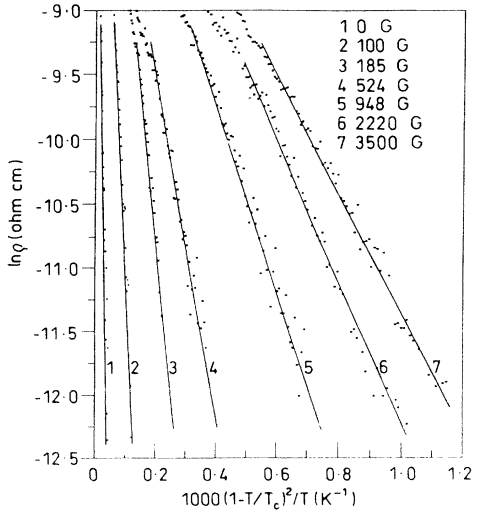

FIG. 8. Arrhenius plot of the magnetoresistivity near T_{c0} for the $Y_{1.2}$ composite.

times smaller than the normal-state resistivity of the bulk sample at 100 K.

A significant point in the Arrhenius plot of the data is that the exponent q can be chosen to be either 1.5 or 2. The only difference between these values is found to be that the higher value of q gives a larger temperature range over which the resistivity data show a straight line fit and therefore, thermally activated behavior. We found the value of $q=2$ to give the best fit and was taken as the optimum value for all the $Y_{1.x}$ composites. The values obtained for the pinning energy $U_0(H)$ using the $Y_{1.2}$ sample are shown in Table III. It should be noted that because of the $(1-t)^q$ factor, the values of $U(H)$ are considerably smaller than the values of $U_0(H)$. Table III also shows the pinning energy values for the Y_{123}, $Y_{1.5}$, and $Y_{1.6}$ composites in the low-temperature region. For the pure Y_{123} sample $\rho_0=(55\pm5)$ $\mu\Omega$ cm, which is very close to the resistivity value at the onset of dissipation (~ 60 $\mu\Omega$ cm) due to the various applied magnetic fields. The high Y_{211} concentration composites, $Y_{1.5}$ and $Y_{1.6}$, show thermally activated flux creep for the resistivity range $\rho(T)/\rho_n=1.7\times10^{-1}$–$10^{-3}$ with $\rho_0=(55\pm1)\times10^{-3}$ and $(6\pm1)\times10^{-2}$ $\mu\Omega$ cm, respectively. The former is almost equal to the normal-state resistivity of the intergranular material of the sample while the latter is three times larger.

It is clear from Table III that the pinning energies, $U_0(H)$, significantly decrease, at each applied magnetic field, as the Y_{211} concentration is increased in the $Y_{1.x}$ composite. This is not unexpected as the results of this study show the decrease of the weak link grain coupling with increased Y_{211} concentration.

In Fig. 9 the magnetic-field-dependent activation energy $U_0(H)$ has been plotted as a function of applied magnetic field for the different $Y_{1.x}$ composites. The results suggest a power-law dependence $U(H)\sim H^{-\alpha}$ for all these composites with $\alpha=0.65$, 0.54, 0.51, and 0.64 for the Y_{123}, $Y_{1.2}$, $Y_{1.5}$, and the $Y_{1.6}$ samples, respectively. The values of α for different composites are very similar and close to 0.5, which are in excellent agreement with those found for $YBa_2Cu_3O_{7-\delta}$ films,[39] $Bi_2Sr_2CaCu_2O_8$ single crystals[35] with magnetic fields perpendicular to the a-b plane.

TABLE III. The pinning energy $U_0(H)$ for several granular $Y_{1.x}$ composites determined from Arrhenius plots of the resistive transition curves near T_{c0}.

Applied magnetic field (G)	Pinning energy $U_0(H)$ (K)			
Composite	Y_{123}	$Y_{1.2}$	$Y_{1.5}$	$Y_{1.6}$
100	1 600 500	45 500	7030	3037
185		19 876	3700	1960
312	901 660	13 225	2511	1060
524		11 300	2102	706
948	431 913	7 200		567
2220	232 019	5 820	1300	450
3500	150 680	4 470	955	

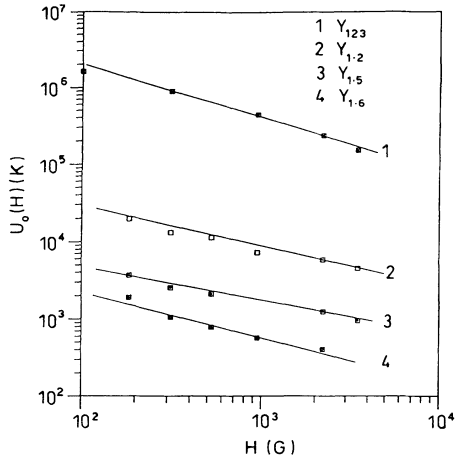

FIG. 9. The magnetic-field dependence of the activation energy $U_0(H)$ for flux creep in the $Y_{1.x}$ composite at temperatures close to T_{c0}. The power-law dependence of $U_0\sim H^{-\alpha}$ has $\alpha=0.5$ for the $Y_{1.2}$ and $Y_{1.5}$ samples and 0.64 for the Y_{123} and $Y_{1.6}$ samples.

CONCLUSIONS

The resistive transition of $Y_{1.x}$ composites have been investigated under various applied magnetic fields at a fixed low transport current density. In the region of the superconducting transition the samples show two distinct sections, a steep part, $\Delta\rho$, which is associated with the onset of superconductivity in the individual superconducting grains and a transition tail, which is due to the weak links coupling the grains. It is found that for the resistive transitions, the ratio of $\Delta\rho$ to the total resistivity of a sample at 100 K, $\Delta\rho/\rho_{100}$, is composition dependent. While this ratio is constant for an individual sample in various magnetic fields up to 4 kG it decreases for the different composites as the Y_{211} concentration is increased. It is also found that for each sample the steep part of the resistive transition remains unchanged with increasing applied magnetic field, whereas the transition tail moves considerably to lower temperatures. This dissipation region has been found to be very sensitive to both transport current and applied magnetic field as the percolation limit is approached. For a fixed, low, transport current, the magnetic-field-induced dissipation region (tail) of the resistive transition for the $Y_{1.x}$ system has been interpreted using the Ambegaokar and Halperin phase-slip model. Good agreement was found between this model and the experimental data using a four-variable fitting procedure. The fitting parameter $C=A/2H$ has been used to estimate the critical current density, at zero temperature, $J_{cj}(0)$, in the grain boundaries for the different composites of the $Y_{1.x}$ system at various magnetic fields.

The magnetic field dependence of the parameter $\gamma(H)$ in the AH model, which is proportional to the activation energy for phase slip, was found to follow a power-law relationship $\gamma(H)\propto H^{-n}$ with $n=0.5$ for pure Y_{123} and 0.3 for the other composites in the range $0<x\leq0.6$. However, for the very-low-temperature region, close to T_{c0}, it

was found that there is a discrepancy between the AH model and the experimental data. It was assumed that the discrepancy may arise from a different dissipative process for this low-temperature region. The resistivity data near T_{c0} were interpreted in terms of the thermally activated flux-creep model and excellent agreement was found. The pinning energy due to the thermally activated process in the flux-line lattice has been determined and the functional dependence of this energy, U_0, for applied magnetic field H was found to follow the well-known form $U_0(H) \propto H^{-\alpha}$ with $\alpha = 0.60 \pm 0.05$ for our samples.

[1]B. Batlogg, T. T. M. Palstra, L. F. Schneemeyer, and J. V. Waszczak, in *Strong Correlation and Superconductivity,* edited by H. Fukuyama, S. Maekawa, and A. P. Malozemoff, Springer Series in Solid State Science, Vol. 89 (Springer-Verlag, Berlin, 1989).

[2]T. T. M. Palstra, B. Batlogg, L. F. Schneemeyer, and J. V. Waszczak, Phys. Rev. Lett. **61**, 1662 (1988).

[3]T. T. M. Palstra, B. Batlogg, R. B. van Dover, L. F. Schneemeyer, and J. V. Waszczak, Appl. Phys. Lett. **54**, 763 (1989).

[4]A. P. Malozemoff, T. K. Worthington, E. Zeldov, N. C. Yeh, M. W. McElfresh, and F. Holtzberg, in *Strong Correlation and Superconductivity* (Ref. 1).

[5]R. Griessen, Phys. Rev. Lett. **64**, 1674 (1990).

[6]P. W. Anderson, Phys. Rev. Lett. **9**, 309 (1962).

[7]Y. B. Kim, C. F. Hempstead, and A. R. Strand, Phys. Rev. Lett. **12**, 145 (1964).

[8]M. Tinkham, Phys. Rev. Lett. **13**, 804 (1964).

[9]Y. B. Kim, C. F. Hempstead, and A. R. Strand, Phys. Rev. **131**, 2486 (1963).

[10]M. R. Beasley, R. Labush, and W. W. Webb, Phys. Rev. **181**, 682 (1969).

[11]J. Bardeen and M. J. Stephen, in *Superconductivity,* edited by R. D. Parks (Dekker, New York, 1969), Chap. 19.

[12]L. F. Schneemeyer, R. B. van Dover, S. H. Glarum, S. A. Sunshine, R. M. Fleming, B. Batlogg, T. Siegrist, J. H. Marshal, J. V. Waszczak, and L. W. Rupp, Nature (London) **332**, 442 (1988).

[13]Y. Iye, S. Nakamura, and T. Tamegai, Physica C **159**, 433 (1989).

[14]K. C. Woo, K. E. Gray, R. T. Kampwirth, J. H. Kang, S. J. Stein, R. East, and D. M. McKay, Phys. Rev. Lett. **63**, 1877 (1989).

[15]S. Kambe, M. Naito, I. Tanaka, and H. Kojima, Jpn. J. Appl. Phys. **28**, L555 (1989); S. Kambe, M. Naito, K. Kitazawa, I. Tanaka, and H. Kojima, Physica C **160**, 243 (1989).

[16]H. Iwasaki, N. Kobayashi, M. Kikuchi, S. Nakajima, T. Kajitani, Y. Synono, and Y. Muto, Physica C **159**, 301 (1989).

[17]R. C. Budhani, D. O. Welch, M. Suenaga, and R. L. Sabatini, Phys. Rev. Lett. **64**, 1666 (1990).

[18]W. K. Kwok, U. Welp. G. W. Crabtree, K. G. Vandervoort, R. Hulscher, and J. Z. Liu, Phys. Rev. Lett. **64**, 966 (1990).

[19]J. R. Clem, Phys. Rev. B **26**, 2463 (1982).

[20]V. Ambegaokar and B. I. Halperin, Phys. Lett. **22**, 1364 (1969).

[21]M. Tinkham and C. J. Lobb, in *Solid State Physics,* edited by H. Ahrenreich and D. Turnbull (Academic, New York, 1989), Vol. 42, p. 91.

[22]M. Tinkham, Phys. Rev. Lett. **61**, 1658 (1988).

[23]A. C. Wright, K. Zhang, and A. Erbil, Phys. Rev. B **44**, 863 (1991).

[24]H. A. Blackstead, D. B. Pulling, P. J. McGinn, and J. Z. Liu, Physica C **174**, 394 (1991).

[25]C. Gaffney, H. Petersen, and R. Bednar, Phys. Rev. B **48**, 3388 (1993).

[26]P. P. Freitas, C. C. Tsuei, and T. S. Plaskett, Phys. Rev. B **36**, 833 (1987).

[27]G. Deutscher and K. A. Müller, Phys. Rev. Lett. **59**, 1745 (1987).

[28]D. H. Kim, K. E. Gray, R. T. Kampwirth, and D. M. McKay, Phys. Rev. B **42**, 6249 (1990).

[29]H. S. Gamchi, Ph.D. thesis, University of New South Wales, Australia, 1994.

[30]S. G. Hassan, K. N. R. Taylor, and G. J. Russell, Physica C **185-189**, 2317 (1991).

[31]S. A. Wolf, D. U. Gubser, W. W. Fuller, J. C. Garland, and R. S. Newrock, Phys. Rev. Lett. **47**, 1071 (1981).

[32]R. F. Voss and R. A. Webb, Phys. Rev. **25**, 3446 (1982).

[33]D. J. Resnick, J. C. Garland, J. T. Boyd, S. Shoemaker, and R. S. Newrock, Phys. Rev. Lett. **47**, 1542 (1981).

[34]D. W. Abraham, C. J. Lobb, M. Tinkham, and T. M. Klapwijk, Phys. Rev. **26**, 5268 (1982).

[35]T. T. M. Palstra, B. Batlogg, R. B. van Dover, L. F. Schneemeyer, and J. V. Waszczak, Phys. Rev. B **41**, 6621 (1990).

[36]D. H. Kim, K. E. Gray, R. T. Kampwirth, K. C. Woo, D. M. McKay, and J. Stein, Phys. Rev. B **41**, 11 642 (1990).

[37]M. Tinkham, *Introduction to Superconductivity* (McGraw-Hill, New York, 1975).

[38]Y. Yeshurum and A. P. Malozemoff, Phys. Rev. Lett. **60**, 2202 (1988).

[39]H. E. Horng, H. H. Sung, B. C. Yao, and H. C. Yang, Physica C **185-189**, 2221 (1991).

[40]R. Gross, P. Chaudhari, D. Dimos, A. Gupta, and G. Koren, Phys. Rev. Lett. **64**, 228 (1990).

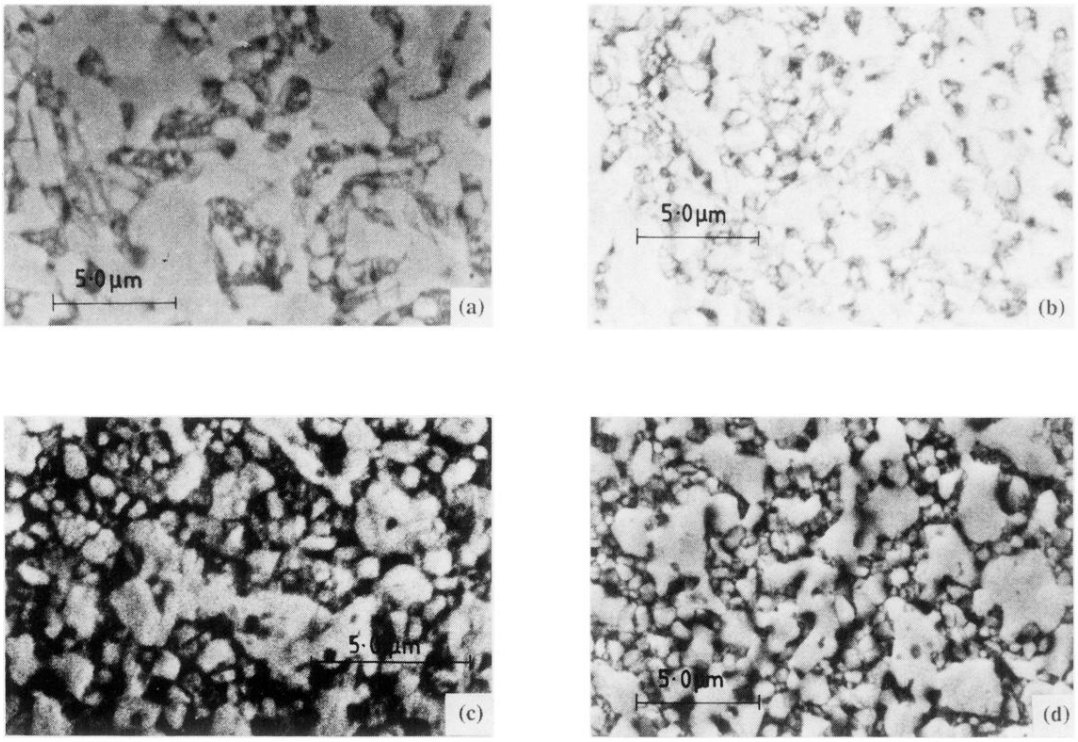

FIG. 2. High-resolution SEM micrographs of (a) the $Y_{1.2}$, (b) the $Y_{1.4}$, (c) the $Y_{1.6}$, and (d) the $Y_{1.775}$ composite samples showing granular decrease of the superconducting cluster size (light areas) as the Y_{211} concentration increases.